crystals

MDPI

Article

Multi-Component Crystals of 2,2′-Bipyridine with Aliphatic Dicarboxylic Acids: Melting Point-Structure Relations

Vhukhudo Nethanani and Eustina Batisai *

Department of Chemistry, Faculty of Science, Engineering and Agriculture, University of Venda, P. Bag X5050, Thohoyandou 0920, South Africa; nethananiv@gmail.com

* Correspondence: Eustina.Batisai@univen.ac.za

Abstract: The aim of the study was to investigate the relationship between the melting point and the supramolecular structure of three multi-component crystals of aliphatic dicarboxylic acids with 2,2′-bipyridine and to investigate the conformations of 2,2′-bipyridine in published multi-component crystals. The crystals were prepared using the solvent evaporation method and were characterized using single-crystal X-ray diffraction (SCXRD), powder X-ray diffraction (PXRD), and differential scanning calorimetry (DSC). The crystal structures were further analyzed using CrystalExplorer, and the results were correlated with the melting points. The results of the conformation analysis of the reported multi-component crystals of 2,2′-bipyridine are also presented.

Keywords: multicomponent crystals; 2,2′-bipyridine; structure-property relations

Citation: Nethanani, V.; Batisai, E. Multi-Component Crystals of 2,2′-Bipyridine with Aliphatic Dicarboxylic Acids: Melting Point-Structure Relations. *Crystals* **2021**, *11*, 1151. https://doi.org/10.3390/cryst11101151

Academic Editor: Alberto Girlando

Received: 11 August 2021
Accepted: 14 September 2021
Published: 22 September 2021

1. Introduction

Co-crystallization is a crystal engineering technique that has been successfully employed in the preparation of new solid forms with improved physical and chemical properties [1,2]. Pharmaceutical co-crystals, in which an active pharmaceutical ingredient with one or more undesirable properties is co-crystallized with a benign compound, are recognized as one of the most successful applications of co-crystallization [3–5]. Structure-property studies form a very important part of co-crystal and pharmaceutical co-crystal research [6–9]. However, the relationship between the supramolecular structure of a co-crystal and some of its physical properties is not yet fully understood. Therefore, understanding this relationship is very important and will ultimately assist in improving the design and synthesis of these compounds.

2,2′-bipyridine (BPY) is a versatile compound that is employed in the preparation of coordination compounds and multi-component crystals. Compounds that have the 2,2′-bipyridine moiety contain a π conjugated system which makes them ideal for use in photochemical devices [10] and nonlinear optical materials [11]. BPY can adopt s-trans or s-cis conformation, and early computational studies showed that the s-trans form is the most stable [12]. In the same paper, the authors also indicated that the unstable s-cis form has an N–C–C–N dihedral angle of 30°. In another study, restricted Hartree Fock (RHF) geometry optimizations were carried out on BPY and monoprotonated BPY (BPY H^+) using the 6–31 G** basis set [13]. It was found that the most stable s-cis BPY has an N–C–C–N dihedral angle of 44.9° while the most stable s-cis monoprotonated form (s-cis BPY H^+) has a dihedral angle of 0°. Using the same basis set, the s-trans BPY was shown to prefer a planar geometry with an N–C–C–N dihedral angle of 180° while the monoprotonated s-trans BPY (s-trans BPY H^+) has an N–C–C–N dihedral angle of 153.7°.

The aim of this study is threefold. Firstly, to prepare multi-component crystals of BPY with aliphatic dicarboxylic acids (Figure 1). Secondly, to investigate the relationship between supramolecular structure and melting point in the resulting crystals. Lastly, to examine the conformation of BPY in the new crystal structures as well as structures deposited in the Cambridge Structural Database (CSD) [14]. BPY was chosen for this

study because of its simplicity. The pyridyl is a good hydrogen bond acceptor, while the carboxylic acid is a good hydrogen bond donor. Therefore, we expected the N···H–O heterosynthon to direct co-crystal formation.

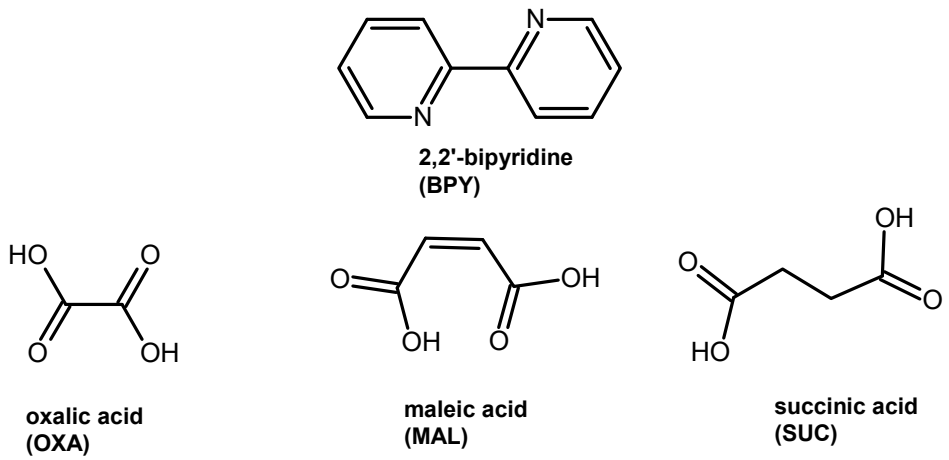

Figure 1. Structures and abbreviations of compounds used in this study.

Herein, we report a melting point–structure analysis of multi-component crystals of BPY with oxalic acid (BPY $H^+ \cdot OXA^-$), maleic acid (BPY $2H^+ \cdot 2MAL^-$), and succinic acid (BPY·SUC), and a CSD conformation analysis of multi-component crystals containing BPY. It was initially intended to include multi-component crystals of glutaric acid and adipic acid in this series; however, the co-crystallization experiments were unsuccessful, and only BPY crystallized in both experiments. A reported co-crystal of BPY and succinic acid (BPY·SUC) [15] was also reproduced in this study, and its structure-property relationship was investigated.

2. Materials and Methods

All chemicals were supplied by Sigma-Aldrich (Burlington, MA, USA) and were used without further purification.

2.1. Preparation of Co-Crystals

Crystals of BPY $H^+ \cdot OXA^-$ and BPY $2H^+ \cdot 2MAL^-$ were prepared by dissolving BPY and the corresponding dicarboxylic acid in a 1:1 molar ratio in methanol. The solvent was allowed to evaporate, and crystals appeared after several days. Crystals of BPY·SUC [15] were prepared following a reported procedure.

2.2. Single-Crystal X-ray Diffraction

Data were collected on the Bruker DUO APEX II diffractometer with graphite-monoch romated MoKα radiation (λ = 0.71073 Å) at 173 K using an Oxford Cryostream 700. Data collection and cell refinement were performed using SAINT-Plus [16], and the space groups were determined from systematic absences using XPREP [17]. Accurate unit cell parameters were refined on all data. The structures were solved using SHELXS-97 [18] and refined using full-matrix least-squares methods in SHELXL-97 [18]. X-Seed [19] was used as an interface to the SHELX programs. Non-hydrogen atoms were refined anisotropically by means of full-matrix least-squares calculation on F^2. Hydroxyl hydrogen atoms were located in the difference electron density map. The hydrogen atoms bound to carbon atoms were placed at idealized positions and refined as riding atoms. Figures were prepared using X-SEED [19] as well as POV-Ray [20]. CCDC deposit numbers 1979404 and 1979405 contain the supplementary crystallographic data for the crystal structures reported in this paper.

2.3. Differential Scanning Calorimetry (DSC)

DSC was used to measure the melting points of the pure compounds as well as the melting points of the multi-component crystals. DSC data were recorded on a PerkinElmer DSC 400. Crystals were dried on a filter paper, weighed, and placed in a vented pan for analysis. Samples were heated at a rate of 10 °C min^{-1} under N_2 atmosphere (flow rate 50 mL min^{-1}). The sample size was varied between 1–2 mg.

2.4. Powder X-ray Diffraction (PXRD)

PXRD data were recorded on a PANalytical XPERT-PRO diffractometer. The diffractometer is equipped with Bragg-Brentano geometry and uses Cu K-α radiation (1.5418 Å) as the incident beam. Intensity data were collected on a flat stage. Samples were gently preground using a mortar and pestle and loaded onto a zero-background sample holder. The samples were scanned between 3° and 50° with a scan step size of 0.017° and a scan speed of 42 s per step. The PXRD patterns of BPY H^+·OXA^-, BPY $2H^+$·$2MAL^-$ and BPY·SUC are shown in Figures S4–S6 in the supplementary material.

3. Results and Discussion

3.1. Differential Scanning Calorimetry

To verify the formation of a new co-crystal or a salt, DSC analysis was performed on the synthesized multi-component crystals (Figures S1–S3). BPY·SUC was also reproduced and its melting point measured. The melting point of BPY H^+·OXA^- is 135.7 °C. This indicates stronger interactions in BPY H^+·OXA^- compared to OXA and BPY. The melting points of BPY $2H^+$·$2MAL^-$ (116 °C) and BPY·SUC (94 °C) are higher than that of BPY but lower than the melting point of the corresponding dicarboxylic acid. This indicates stronger intermolecular interactions in the multi-component crystals compared to those in **BPY** but weaker than the interactions in the corresponding dicarboxylic acid.

3.2. Single-Crystal X-ray Diffraction

3.2.1. BPY H^+·OXA^-

Slow evaporation of a methanol solution of oxalic acid and 2,2′-bipyridine in a 1:1 molar ratio yielded crystals of BPY H^+·OXA^-. BPY H^+·OXA^- crystallizes in the monoclinic space group $P2_1/c$ with one BPY H^+ and one OXA^- in the asymmetric unit. The structure is a salt, i.e., a proton is transferred from oxalic acid to 2,2′-bipyridine. The N toms in the BPY H^+ are in the s-cis conformation. BPY H^+ and OXA^- molecules interact via intermolecular charge assisted hydrogen bonds (N–$H^+\cdots{}^-$O) as well as C–H···O (C8–H8···O16 and C9–H9···O15) interactions forming 1D chains running along the *c* axis (Figure 2a). The ID chains interact with each other via C–H···O interactions (C10–H10···O15 and C11–H11···O18) as well as C···O interactions (C11···O18 = 3.080 Å). OXA^- molecules interact with each other via O–H···O interactions while the BPY H^+ molecules interact with each other along the *b* axis via π···π interactions (centroid to centroid distance = 3.60 Å). The packing diagram viewed down the *b* axis is shown in Figure 2b. Crystallographic data are given in Table 1, and hydrogen bond and short contact details are given in Table 2.

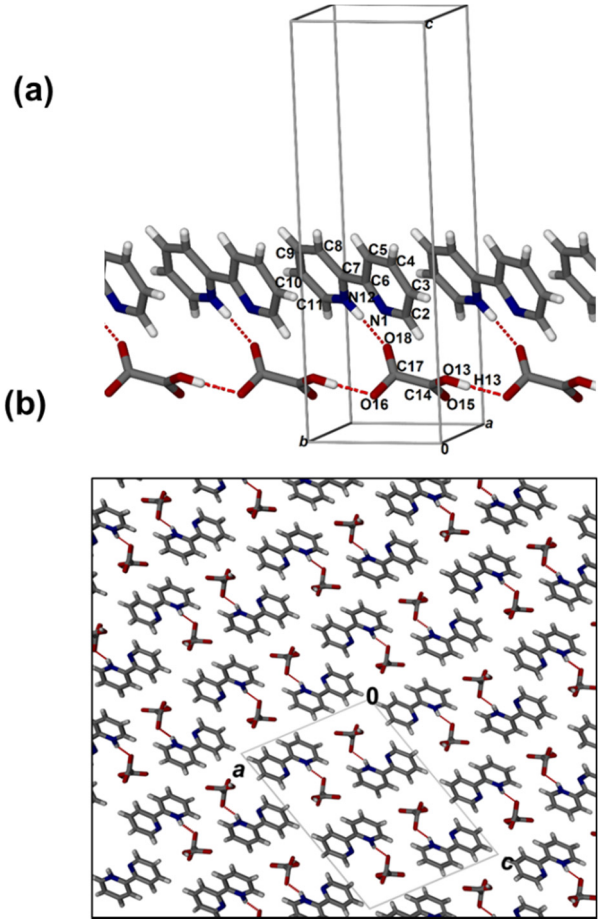

Figure 2. (**a**) A 1D chain of BPY $H^+ \cdot OXA^-$ formed by the interaction between BPY $H^+ \cdot$and OXA^- and (**b**) the packing diagram of BPY $H^+ \cdot OXA^-$ viewed down the *b* axis.

Table 1. Selected crystallographic data for BPY $H^+ \cdot OXA^-$ and BPY $2H^+ \cdot 2MAL^-$.

	BPY $H^+ \cdot OXA^-$	**BPY $2H^+ \cdot 2MAL^-$**
CCDC number	1979405	1979404
Molecular formula	$C_{12}H_{10}N_2O_4$	C_{18} H_{14} N_2 O_8
Formula weight	246.22	386.31
Temperature (K)	173	173
Crystal system	Monoclinic	Monoclinic
Space group	$P2_1/c$	$P2_1/n$
a/Å	12.225 (2)	12.038 (4)
b/Å	5.3046 (9)	5.4644 (18)
c/Å	17.680 (3)	13.068 (4)
α/°	90	90
β/°	106.409 (3)	90.207 (7)°
γ/°	90	90
Volume (Å^3)	1099.9 (3)	859.6 (5)
Z	4	2
ρ (g cm^{-3})	1.487	1.492
μ (mm^{-1})	0.114 mm^{-1}	0.120
Limiting indices (*hkl*)	±16; ±7; ±23	±16; 6, −7; ±17
Reflections collected/unique	16779/2730	6525/2129
R_{int}	0.0298	0.0479
Final R indices [$I > 2\sigma(I)$]	R_1 = 0.0373, wR_2 = 0.0992	R_1 = 0.0668, wR_2 = 0.1709

Table 2. Hydrogen bond details and short contacts for BPY $H^+ \cdot OXA^-$ and BPY $2H^+ \cdot 2MAL^-$.

D–H···A	D–H (Å)	H···A (Å)	D–H···A (Å)	∠D–H···A (°)
BPY $H^+ \cdot OXA^-$				
N12–H12···O18 [i]	0.88	1.87	2.6697 (5)	150
O13–H13···O16 [i]	0.84	1.68	2.5170 (4)	172
C8–H8···O16 [ii]	0.95	2.50	3.4408 (6)	173
C9–H9···O15 [ii]	0.95	2.43	3.2465 (6)	143
C10–H10···O15 [iii]	0.95	2.34	3.2810 (6)	169
C11–H11···O18 [iv]	0.95	2.39	3.0801 (5)	129
BPY $2H^+ \cdot 2MAL^-$				
N1–H1···O9 [v]	1.03	1.99	2.9688 (10)	158
C3–H3···O7 [vi]	0.95	2.59	3.5369 (12)	177
C5–H5···N1 [vii]	0.95	2.38	3.3046 (11)	166

Symmetry codes: [(i)] $x, -1+y, z$, [(ii)] $x, 3/2-y, 1/2+z$, [(iii)] $1-x, 1/2+y, 1/2-z$, [(iv)] $1-x, 1/2+y, 1/2-z$, [(v)] $1-x, 1-y, 1-z$, [(vi)] $-1/2+x, 1/2-y, -1/2+z$, [(vii)] $-1+x, -1+y, z$.

3.2.2. BPY $2H^+ \cdot 2MAL^-$

Crystals suitable for single-crystal X-ray diffraction were grown by the solvent evaporation of a methanol solution of maleic acid and 2,2′-bipyridine. BPY $2H^+ \cdot 2MAL^-$ crystallizes in the monoclinic space group $P2_1/n$. The asymmetric unit consists of half a molecule of BPY $2H^+$ and a complete molecule of MAL^-. A proton is transferred from the carboxylic acid group of MAL to the nitrogen of BPY. The BPY $2H^+$ adopts a trans planar confirmation with an N–C–C–N dihedral angle of 180°. The BPY $2H^+$ ring is disordered over two positions; however, the disorder could not be modeled; therefore, only the highest populated orientation was modeled at full occupancy. BPY $2H^+$ and MAL^- are linked into 1D chains via intermolecular N–$H^+ \cdots {}^-$O charge assisted hydrogen bonds between the BPY $2H^+$ and the MAL^- as well as O···O interactions between the MAL^- anions (Figure 3a). There is a further intramolecular hydrogen bond on maleate ions. Neighboring 1D chains interact with each other via C–H···O interactions (C3–H3···O7) as well as C···O interactions (C4···O14 = 3.122 Å). Figure 3b shows the packing diagram of BPY $2H^+ \cdot 2MAL^-$ viewed down the *b* axis. Crystallographic data are given in Table 1, and hydrogen bond and short contact details are given in Table 2.

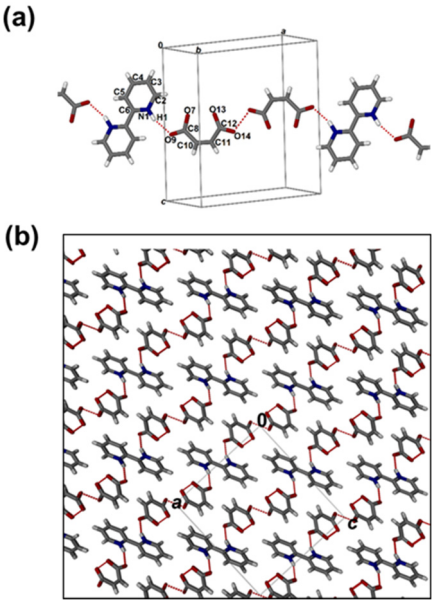

Figure 3. (**a**) 1D chain of BPY $2H^+ \cdot 2MAL^-$ formed by the interaction between BPY $2H^+$ and MAL^- and (**b**) The packing diagram of BPY $2H^+ \cdot 2MAL^-$ viewed down the *b* axis.

3.3. Hirshfeld Surface Analysis

To determine the type and quantity of intermolecular interactions in each structure, the program CrystalExplorer was used to generate 2D fingerprint plots [21]. The 2D fingerprint plots were generated on BPY, BPY H^+, BPY $2H^+$ in BPY·SUC, BPY H^+·OXA^- and BPY $2H^+$·$2MAL^-$, respectively. The 2D fingerprint plots for the O···H, H···H, C···H and N···H interactions are shown in Figure 4 while the 2D fingerprint plots for the C···C, C···N and C···O interactions are shown in Figure S7. Percentage contributions of the interactions as well as the melting points of the structures are given in Table 3. The melting points of the compounds follow the order; BPY H^+·OXA^- > BPY $2H^+$·$2MAL^-$ > BPY·SUC. Generally, strong intermolecular interactions result in a high melting point, and weak intermolecular interactions result in a low melting point. O···H interactions contribute 16.5% in BPY·SUC, 31.3% in BPY $2H^+$·$2MAL^-$ and 28.3% in the BPY H^+·OXA^-. BPY $2H^+$·$2MAL^-$ has a slightly higher percentage of O···H interactions compared to BPY H^+·OXA^-; however, the closest O···H interactions distance is shorter (1.87 Å) in BPY H^+·OXA^- than in BPY $2H^+$·$2MAL^-$ (2.14 Å). The percentage contributions of H···H interactions follow the order: BPY·SUC > BPY $2H^+$·$2MAL^-$ > BPY H^+·OXA^-. The multicomponent crystal having the lowest percentage of H···H interactions has the highest melting point. BPY·SUC has the highest percentage of H···H interactions; this may indicate a less dense packing arrangement in the structure compared to BPY $2H^+$·$2MAL^-$ and BPY H^+·OXA^-. The percentage contributions of C···H interactions follow the order; BPY H^+·OXA^- > BPY·SUC > BPY $2H^+$·$2MAL^-$. N···H interactions also contribute significantly to the total Hirshfeld surface in BPY H^+·OXA^- and BPY·SUC. The highest percentage of N···H interactions are observed in BPY·SUC with the shortest contact distance of 1.88 Å. The sum of the percentage contributions of aromatic interactions (C···C, C···N and C···O) is highest in the BPY H^+·OXA^- structure followed by the BPY $2H^+$·$2MAL^-$ then BPY·SUC.

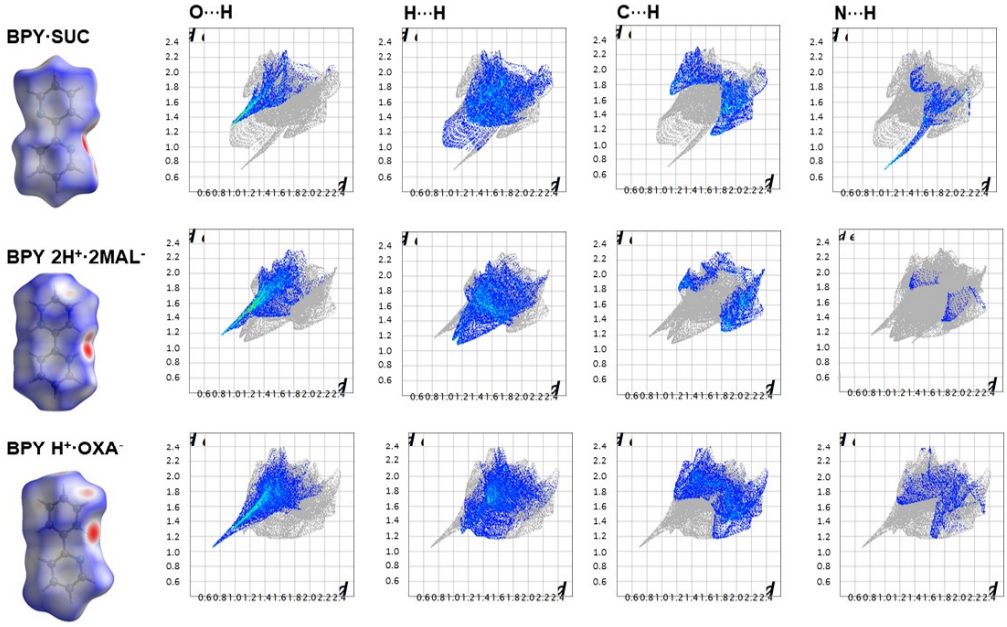

Figure 4. 2D fingerprint plots of BPY·SUC, BPY $2H^+$·$2MAL^-$ and BPY H^+·OXA^- showing the O···H, H···H, C···H, and N···H interactions.

Table 3. Percentage contributions of the main interactions in BPY $H^+ \cdot OXA^-$, BPY $2H^+ \cdot 2MAL^-$ and BPY·SUC as well as the melting points of the compounds.

Compound	O···H (%)	C···H (%)	N···H (%)	H···H (%)	Aromatic (%)	Other (%)	Melting Point (°C)
BPY·SUC	16.5	23.9	11.2	39.6	8.6	0.2	93.4
BPY $2H^+ \cdot 2MAL^-$	31.3	18.2	1.9	35.3	10.6	2.7	117.0
BPY $H^+ \cdot OXA^-$	28.3	24.8	7.1	26.9	12.1	0.8	135.7

3.4. Cambridge Structural Database (CSD) Conformational Analysis of the 2,2′-Bipyridine

Given that the 2,2′-bipyridine can adopt an s-cis or an s-trans conformation, we thought it would be interesting to analyze the conformation of 2,2′-bipyridine in the solid state in published multi-component crystals. Therefore, three searches were conducted separately on the CSD (version 5.51, March 2020) (Figures S8–S10) using the search fragments depicted in Figure 5. The first search was conducted using BPY. The search produced 78 hits. Of the 78 hits, only 10 adopt the s-cis geometry, and the remaining 68 adopt the s-trans geometry. Of these 68 that adopt the s-trans geometry, 46 have an *s*-trans planar configuration with torsion angles of 180°. The rest have torsion angles between 143° and 179°. The second search was conducted on a monoprotonated 2,2′-bipyridine fragment (BPY H^+). The search produced 57 hits, with all the monoprotonated 2,2′-bipyridine, except 1 (CCDC ref code OGAVOJ), adopting an *s*-cis conformation. The third search was conducted on a biprotonated 2,2′-bipyridine (BPY $2H^+$). This search produced 14 hits, and of these, only 2 adopt an s-cis conformation (both with CCDC ref code KAPKES). The other 12 adopt an s-trans conformation in which 4 are s-trans planar. In the present study, the monoprotonated 2,2′-bipyridine in the multi-component crystal of BPY $H^+ \cdot OXA^-$ adopts an s-cis conformation with a dihedral angle of 5.7°, whilst the 2,2′-bipyridine in BPY·SUC structure adopts an s-trans planar conformation with an N–C–C–N of 180°.

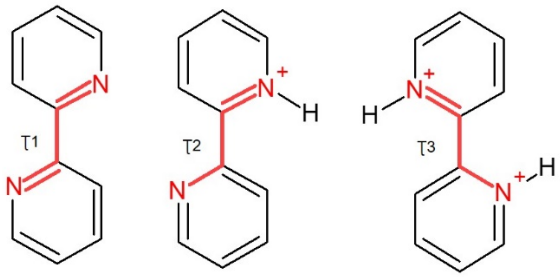

Figure 5. Schematic representation of the search fragments showing the torsion angles. T1, T2 and T3 represent the torsion angles for BPY, BPY H^+, and BPY $2H^+$, respectively.

4. Conclusions

In summary, two new multi-component crystals containing 2,2′-bipyridine and maleic acid (BPY $2H^+ \cdot 2MAL^-$) and, 2,2′-bipyridine and oxalic acid (BPY $H^+ \cdot OXA^-$) were synthesized and characterized. The intermolecular interactions in the two new salts, as well as the reported co-crystal, bipyridine and succinic acid (BPY·SUC), were analyzed using CrystalExplorer. It was found that BPY $H^+ \cdot OXA^-$ has the highest percentage of O···H and C···H interactions and the highest melting point compared to the other two multi-component crystals. A search conducted on the CSD indicated that 59% of BPY in multi-component crystal structures adopt the s-trans planar conformation while in the multi-component crystal structures of monoprotonated 2,2′-bipyridine and biprotonated 2,2′-bipyridine 98% of the BPY H^+ adopt the s-cis geometry and 85% of the BPY $2H^+$ adopt the s-trans, respectively.

Supplementary Materials: The following are available online at https://www.mdpi.com/article/10.3390/cryst11101151/s1, Figure S1. DSC thermogram of BPY $H^+ \cdot OXA^-$; Figure S2. DSC thermogram of BPY $2H^+ \cdot 2MAL^-$; Figure S3. DSC thermogram of BPY·SUC; Figure S4. PXRD patterns for simulated and as-synthesized BPY·SUC; Figure S5. PXRD patterns for simulated and as-synthesized BPY $H^+ \cdot OXA^-$; Figure S6. PXRD patterns for simulated and as-synthesized BPY $2H^+ \cdot 2MAL^-$; Figure S7. 2D fingerprint plots of BPY·SUC, BPY $2H^+ \cdot 2MAL$ and BPY $H^+ \cdot OXA^-$ showing the C···C, C···N and C···O interactions; Figure S8. Results of CSD search on the BPY molecule; Figure S9. Results of CSD search on monoprotonated BPY; Figure S10. Results of CSD analysis on diprotonated BPY.

Author Contributions: Methodology, validation, formal analysis, experiment and material, characterization, writing-original draft preparation; V.N. Conceptualization, writing-review and editing, supervision, project administration, and funding acquisition; E.B. All authors have read and agreed to the published version of the manuscript. V.N. sadly passed away in April 2018 after the drafting of the original paper.

Funding: The National Research Foundation of South Africa (Thuthuka grant number 113224) and the University of Venda Research and Publications Committee are acknowledged for funding this project.

Conflicts of Interest: The authors declare no conflict of interest.

References

1. Bavishi, D.D.; Borkhataria, C.H. Spring and parachute: How cocrystals enhance solubility. *Prog. Cryst. Growth Charact. Mater.* **2016**, *62*, 1–8. [CrossRef]
2. Karimi-Jafari, M.; Padrela, L.; Walker, G.M.; Croker, D.M. Creating cocrystals: A review of pharmaceutical cocrystal preparation routes and applications. *Cryst. Growth Des.* **2018**, *18*, 6370–6387. [CrossRef]
3. Shan, N.; Zaworotko, M.J. The role of cocrystals in pharmaceutical science. *Drug Discov. Today* **2008**, *13*, 440–446. [CrossRef] [PubMed]
4. Qiao, N.; Li, M.; Schlindwein, W.; Malek, N.; Davies, A.; Trappitt, G. Pharmaceutical cocrystals: An overview. *Int. J. Pharm.* **2011**, *419*, 1–11. [CrossRef] [PubMed]
5. Thakuria, R.; Delori, A.; Jones, W.; Lipert, M.P.; Roy, L.; Rodríguez-Hornedo, N. Pharmaceutical cocrystals and poorly soluble drugs. *Int. J. Pharm.* **2012**, *453*, 101–125. [CrossRef] [PubMed]
6. Suresh, A.; Minkov, V.S.; Namila, K.K.; Derevyannikova, E.; Losev, E.; Nangia, A.; Boldyreva, E.V. Novel synthons in sulfamethizole cocrystals: Structure−property relations and solubility. *Cryst. Growth Des.* **2015**, *15*, 3498–3510. [CrossRef]
7. Batisai, E.; Ayamine, A.; Kilinkissa, O.E.Y.; Báthori, N.B. Melting point-solubility-structure correlations in multicomponent crystals containing fumaric or adipic acid. *CrystEngComm* **2014**, *16*, 9992–9998. [CrossRef]
8. Batisai, E. Multicomponent crystals of anti-tuberculosis drugs: A mini-review. *RSC Adv.* **2020**, *10*, 37134–37141. [CrossRef]
9. Kilinkissa, O.E.Y.; Govender, K.K.; Báthori, N.B. Melting point-solubility-structure correlations in chiral and racemic model cocrystals. *CrystEngComm* **2020**, *22*, 2766–2771. [CrossRef]
10. Meyer, T.J. Chemical approaches to artificial photosynthesis. 2. *Acc. Chem. Res.* **1989**, *22*, 163–170. [CrossRef]
11. Long, N.J. Organometallic Compounds for Nonlinear Optics–The Search for En-light-enment! *Angew. Chem. Int. Ed. Engl.* **1995**, *34*, 21–38. [CrossRef]
12. Galasso, V.; De Alti, G. MO calculations on the preferred conformation and electronic structure of phenyl-derivatives of pyrrole, furan and thiophene. *Tetrahedron* **1971**, *27*, 4947–4951. [CrossRef]
13. Howard, S.T. Conformers, energetics, and basicity of 2,2′-bipyridine. *J. Am. Chem. Soc.* **1996**, *118*, 10269–10274. [CrossRef]
14. Groom, C.R.; Bruno, I.J.; Lightfoot, M.P.; Ward, S.C. The Cambridge structural database. *Acta Crystallogr. Sect. B Struct. Sci. Cryst. Eng. Mater.* **2016**, *72*, 171–179. [CrossRef] [PubMed]
15. Barnett, S.A.; Tocher, D.A.; Price, S.L.; Mohamed, S.; Braun, D.E.; Issa, N.; Copley, R.C.B. Screening for cocrystals of succinic acid and 4-aminobenzoic acid. *CrystEngComm* **2012**, *14*, 2454. [CrossRef]
16. Bruker. *SAINT-Plus (Including XPREP)*, Version 7.12; Bruker AXS Inc.: Madison, WA, USA, 2003.
17. Bruker. *XPREP2*, Version 6.14; Bruker AXS Inc.: Madison, WA, USA, 2003.
18. Sheldrick, G.M. A short history of SHELX. *Acta Crystallogr. Sect. A Found. Crystallogr.* **2008**, *64*, 112–122. [CrossRef] [PubMed]
19. Barbour, L.J. X-seed–A software tool for supramolecular crystallography. *J. Supramol. Chem.* **2001**, *1*, 189–191. [CrossRef]
20. Persistence of Vision Pty. Ltd. Persistence of Vision Raytracer (Version 3.6). 2004. Available online: http://www.povray.org/download/ (accessed on 11 August 2021).
21. Spackman, M.A.; Jayatilaka, D. Hirshfeld surface analysis. *CrystEngComm* **2009**, *11*, 19–32. [CrossRef]